Dynamical Assessment of Structural Damage Using the Continuity Statistic

Linda Moniz[1] Louis Pecora[2] Jonathan Nichols[3] Michael Todd[4]
J.R. Wait[5]

March 25, 2003

[1]Corresponding author. Code 6340 Naval Research Laboratory, Washington, DC 20375 USA. Phone (202) 767 6259, fax (202) 767 1697, email moniz@anvil.nrl.navy.mil. This project was supported by an ONR-ASEE Fellowship and a 6.1 Navy ARI

[2]Code 6340, Naval Research Laboratory, Washington, DC 20375 USA

[3]Code 5673, Naval Research Laboratory, Washington, DC 20375 USA. This project was supported by an NRC Fellowship and a 6.1 Navy ARI

[4]Department of Structural Engineering, University of California, San Diego, La Jolla, CA 92093-0085

[5]Weapons Response Group (ESA-WR) Los Alamos National Laboratory, MS T006, Los Alamos, NM 87545

Abstract

Recent work by Nichols et al [8] and Pecora et al[22] have shown that steady-state dynamic analysis of structural health exhibits large advantages over transient vibrational analysis. A geometric representation of system dynamics can be used to extract information about a structure's response to sustained excitation. Analysis of various features of the geometric representation can be used to describe the degree to which the dynamics have been altered by damage. Here, the feature we employ is the "continuity test," a statistical test first described by Pecora, Carroll and Heagy [14]. This test measures the probability that a continuous function exists from one geometric object to another. In this implementation, we formulate a new null hypothesis which serves to make the test less sensitive to noise in the data than the original test. Using experimental data from an excited three-story aluminum frame structure with multiple sensors at the joints, we show that the continuity test can be used not only to detect, but also in some cases to localize damage to particular joints in the frame structure.

Key Words: Nondestructive structural health evaluation, damage localization, attractor, lyapunov exponents, continuity test, filtered Lorenz signal

0.1 Introduction

Assessing the functional health of a given structure is an important concern in many civilian and military communities. Human inspection techniques and fixed maintenance and replacement schedules have been the historical norm. However, recent advancements in non-destructive evaluation of structures may make it possible to adapt automated technologies and in doing so reduce manpower and costs associated with maintenance.

Currently, major approaches include ultrasonic (e.g.[23]), acoustic (e.g. [19]), wave propagation and thermal imaging [17], X-ray radiography [20] and eddy-current methods[1]. These techniques have proven to be quite useful [5] in particular damage scenarios, but they are primarily local techniques. Thus, it is necessary to know that damage has possibly occurred and to also know where to look for it. In addition, many of these techniques are impractical to apply to large-scale structures. In the vibration-based techniques, the structure is excited, and the interrogator then looks for features of the response that identify and localize the damage. Traditionally, the features have been derived from modal analyses of the structure such as resonant frequencies and mode shapes [6, 12, 15, 24, 18].

Recently, the use of deterministic dynamics (see Todd et al [22]) has shown advantages over previous modal analyses in both sensitivity to low levels of damage and resistance to noise. The experimenter excites the structure with a chaotic(deterministic) signal; the structure acts as a linear filter. In the case of stochastic excitation, the structure's steady-state response is too high-dimensional for efficient calculation of features, and at the other extreme, for example a sinusoidal excitation, the response is too low-dimensional to observe changes in features even with significant damage to the structure. With a properly tuned chaotic signal, the structure's steady-state response can be sufficiently low dimensional to allow computation of features, and sufficiently high dimensional that the changes to the dynamics can be observed. The deterministic-signal approach takes advantage of the ways in which the structure's filtering of the chaotic input changes as damage to the structure occurs. Moreover, local changes in the structure produce a global response to the input signal; it is not necessary to know where the damage occurred or if it occurred in order to detect it.

The work by Nichols, Todd et al [8] describes a feature that used statistical prediction of a damaged structure's response based on data taken from the structure in a healthy condition. Here, we also analyze the time series from the filtered response, but we take a somewhat different approach. Like Todd, et al [22] we embed the time series in an appropriate dimension in order to reconstruct a geometric object that represents the state space of the dynamical system. However, in this work we isolate subspaces of the geometric object and compare them as they are reconstructed from the filtered responses in several damage scenarios. This approach serves to both identify damage to the structure and to localize the damage.

We will first describe the dynamical theory behind the experiments. Then we will provide a detailed explanation of the continuity test and its application to the experimental data. Following that, the next section describes the physical configuration of the experiments. We note at this time when the data from the experiments was received, we did not know the damage location or extent in each scenario (other than identification of a scenario in which the structure was undamaged). Thus, the identification and localization of damage was done as a blind test of the method.

0.2 Steady-State Dynamics and Structural Response to Chaotic Excitation

We now turn to the description of a dynamical system and its use in excitation of a structure.

Consider a nonlinear function $f(x) : \mathbf{X} \to \mathbf{X}$, where we are interested in the evolution $f^n(x)$ of points $x \in X$, for $n \in \mathcal{Z}$. After a period of transient behavior, the iterates of x under f settle into a steady-state. This is the so-called attractor of f in phase space. This attractor can be thought of as the object which all trajectories will approach. We note that although the attractor is embedded in phase space which has dimension equal to the dimension of X, the attractor itself may actually be lower-dimensional. For example, the familiar Henon attractor,

$$f(x, y) = (a - x^2 + by, x) \tag{1}$$

can exhibit a single fixed point, zero dimensional attractor ($a = -.09, b = .4$), seen in figure 1, or an attractor with dimension d such that $1 \leq d < 2$ (e.g. $a = 1.2, b = .4$), as seen in figure 2.

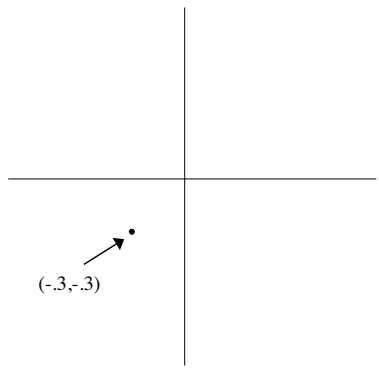

Figure 1: A single fixed point at $(-.3, -.3)$ for parameter values $a = -.09$, $b = .4$ of the Henon Map (equation 1)

We note that it is possible to find a relatively low-dimensional nonlinear function that exhibits complicated behavior, as seen for example in figure 2. It is possible to specify the type of long-term behavior (as we saw above) of the system by choice of parameters.

Now consider applying a linear filter to a nonlinear function. Let the linear filter be the matrix A. Let the nonlinear function be $f : \Re^3 \to \Re^3$ be written as $x_n := f^n(x)$ Thus, we have the following slaved dynamical system:

Figure 2: A fractal attractor for parameter values $a = 1.2$, $b = .4$ of the Henon Map (equation 1). This picture was produced using *Dynamics* [25]

$$y_{n+1} = Ay_n + x_n \tag{2}$$

The input function is unchanged by the filter. However, the slaved system $\{y_n\}$, is determined by the filtering of the base signal $\{x_n\}$ (the drive signal). This is an example of an Infinite Impulse Response (IIR) filter; the series y_n is affected by the entire time history of y. In practice, the dynamical system f is not directly observable; we instead have an observation function $h : X \to \Re$. Then we must include $h(x_n)$ in an appropriate dimension. Let H be the observation function h composed with the inclusion to $\Re^p$. This function H can be thought of as an appropriate coupling function. Thus, we have

$$y_{n+1} = Ay_n + H(x_n) \tag{3}$$

$$x_n = f(x_{n-1}) \tag{4}$$

The stability of any dynamical system is described by its Lyapunov exponents. The Lyapunov exponents describe the average rate of growth or decay of a perturbation to the dynamical system in each phase space direction. In the case of a linear function, the Lyapunov exponents are the logarithms of the moduli of the characteristic values (i.e. the characteristic exponents). We say that such a system is *stable* if all of the characteristic values lie inside the unit circle. In the case of an IIR filter, as long as A is stable, the Lyapunov exponents of the IIR filter are simply the characteristic exponents of A together with the Lyapunov exponents of f (see, e.g. Davies and Campbell [4]). The stability of the entire system depends on the filter A [4, 3]. In a practical situation, all filters provided by linear structures are stable.

The phase space of the filtered signal exists in a space with dimension dependent on the dimension of the drive signal and the dimension of the filter. However, in an experimental setting, a time series of measurements of some function of the filtered signal is the only available quantity. In this case, the phase space of the attractor can be reconstructed using a time-series of the observed quantity. It has been shown that the reconstructed attractor is a faithful representation of the original attractor [16]. Such a reconstruction is termed a time-series embed-

ding. If the observable quantity is denoted $g(n) = (g(1), g(2) \ldots, g(N))$ recorded at discrete times n, we reconstruct the attractor as follows:

Take a delay time T and an embedding dimension m. Then the reconstructed phase-space vector $R(n)$ is the following for any time n:

$$R(n) = (g(n), g(n+T), \ldots, g(n+(m-1)T)). \tag{5}$$

The delayed copies of g are sometimes referred to as pseudo-state vectors. The time delay T and embedding dimension m are determined by examining the time-series itself. For the time delay, one determines the amount of new information given by adding another coordinate with time delay T, as T varies. If T is too short, the observations are too close in time to add any additional phase-space information. If T is too long, the observations are too far apart to be relevant to each other. For this application, the autocorrelation function of the time series was examined and the delay T was chosen to coincide with the loss of 2/3 of the autocorrelation. Often the mutual-information function [7] is used to find a suitable time delay, but the mutual information function can occasionally give falsely negative results [13]. The embedding dimension can be determined by using a false nearest-neighbor technique [10]. In this technique embedding dimensions are added one at a time until false nearest-neighbors - vectors that are close in a smaller dimension, but not close in a larger dimension - are eliminated. With the time delay T and embedding dimension m chosen, we can now use the reconstructed attractor to analyze characteristics of the dynamical system.

In this application, there were multiple time series corresponding to the output signals at 3 of the joints. The false-nearest neighbor technique can still be employed to find an appropriate embedding dimension [2]. The work by Boccaletti et al [2] described time series that were weakly coupled. In this experiment, we encountered time series that were strongly coupled, due to the presence of the drive signal. We modified the method used in Boccaletti et al to add time series one at a time, and in different combinations in order to determine if including all of the time series are necessary to adequately reconstruct the attractor. See also [11] to see another use of the false-nearest neighbor method for multiple strongly coupled time series.

The attractor is usually reconstructed by considering all state-space variables and reconstructing the entire phase space of the dynamical system. In this case, we noted during the false nearest-neighbor examination that the addition of the time series from additional joints' sensors did not increase the embedding dimension of the state-space. This shows that addition of another joints' time series provides redundant information; the drive signal forces a relationship between the reponse signals. Since the response signals are just linearly filtered drive signals, it is likely that this relationship is continuous. Thus, there was some evidence to suggest a continuous function exists between the geometric objects that are reconstructed from the joints' sensor time-series. We reconstructed an attrac-

tor from the x-data from each joint; we then compared the attractors reconstructed from the joints to each other to see if geometric changes occurred over the 6 scenarios.The next problem we encounter is how to determine geometric changes in attractor reconstructions.

0.3 The Continuity Test

Given time-delay embeddings of two different geometric objects reconstructed from time series data, it is often important to find a functional relationship between the two objects. For instance, in the presence of noisy data from the reconstruction of one object, can we say if it is essentially identical to another object? Proving or disproving the existence of a continuous function between two such objects can be a powerful tool for analysis of nonlinear behavior.Given a proposed function $F : X \to Y$ the mathematical definition of continuity at a point $x(t) \in X$ is stated as follows: For all $\epsilon > 0$, $\exists \delta > 0$ such that if $\|x(t_i) - x(t_j)\| < \delta$, then $\|F(x(t_i)) - F(x(t_j))\| < \epsilon$. The geometric meaning of this statement is illustrated in figure 3.

If we let the input to the function be designated as the source and the output designated as the target, then for an arbitrarily small set in the target, a set in the source can be found for which all points map to the set in the target. Thus, we see that points that are close to each other in the source map to points that are close to each other in the target. The 'closeness' is the relationship between δ and ϵ.

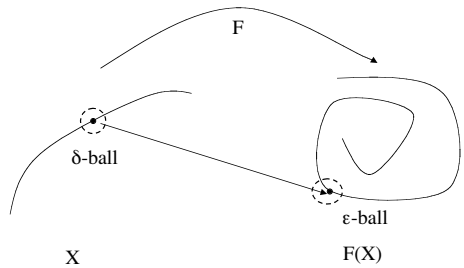

Figure 3: Points from the δ-ball on the left map to the ϵ-ball on the right

For a theoretical geometric object the analytic definition is clear. However, translating the mathematical $\epsilon - \delta$ definition of continuity to a time-series reconstruction setting raises two important questions:

1. How can potentially noisy, finite data yield a reasonable definition of continuity either at a point or on an entire geometric object?

2. How can such a definition be translated to a meaningful and reliable statistic regarding the absence or presence of a continuous function?

Three unrelenting facts, therefore, seem to create an impasse with finite data. The first is that ϵ cannot be made to go to zero. Thus, some finite but small ϵ that still indicates continuity will have to be determined. More-

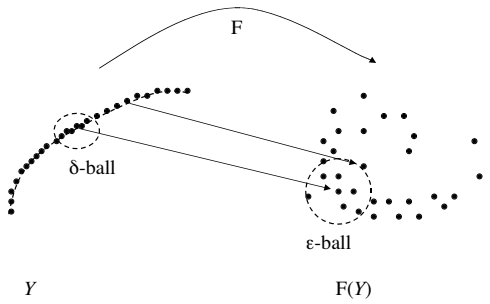

Figure 4: An ϵ and δ may be found but ϵ may be large. Noise may force some points from the δ-ball to be outside the ϵ-ball.

over, for some x, there may be ϵ for which δ can be found even if there is no continuous F. Secondly, only a finite number of points $x \in X$ can be checked for continuity. Lastly, in the presence of noise, even for an obviously continuous F (e.g. an identity function), all points from a δ-ball may not map to the corresponding ϵ-ball. For example, see figure 4.

These issues cannot be ignored, but we can remove the impasse by creating a statistical criterion for continuity that is consistent with the $\epsilon - \delta$ definition but is difficult to fulfill if there is no continuous functional relationship.

We begin with two time series reconstructions, denoted X and Y. The space X will be denoted the source, Y the target (or image). We formulate the continuity test as follows.

Theoretically, we would choose an ϵ as in the formal definition. We find the $\epsilon-$ball around the point y in the space Y. We then take progressively smaller $\delta-$ balls around the corresponding point $x \in X$ that maps to $y \in Y$ until all of the points in the $\delta-$ball are mapped into the $\epsilon-$ball. However, because of the above issues, we need instead to apply a statistical criterion which will reject or accept the $\delta-$ball as passing the continuity test for this ϵ. For this, we formulate a null hypothesis.

The null hypothesis assumes that points $x(t_j)$ from any δ-ball will have probability .5 of $y(t_j)$'s being in the ϵ-ball, regardless of the size of the ϵ-ball. To reject the null hypothesis , we require a 95% confidence interval. If n points are in any δ-ball, the probability of m or more of these points' images in the ϵ-ball must be $< .05$ to reject the null hypothesis.

This null hypothesis essentially assumes that points from the given δ-ball map to points in the ϵ-ball by a coin flip. In order to reject the null(equivalently, to *accept* the $\delta-$ball as passing the continuity test for this ϵ), we must lie in the tail of the binomial distribution. Thus, we must have 95% confidence that the points from the δ-ball did *not* map to the ϵ ball by guessing.

This differs from the null hypothesis described in [14]. To account for noise, our null hypothesis allows some points from the δ-ball to map outside the ϵ-ball but requires 95% confidence; the probability of rejecting the null hypothesis lies in the tail of the binomial distribution. We formulate the statistic to be based not on the acceptance or rejection of the null hypothesis, but on the *minimum* ϵ that can be used to reject the null hypothesis at each point. We call this value ϵ^*. The corresponding δ for which we have rejection of

the null will be termed δ^*. Thus, the statistic can give some idea as to the scaling of any possible functional relationship by looking at the average of ϵ^* compared to δ^* given by the data.

To compute the continuity statistic, N test points $x(t_i)$ are chosen at random times from X. This serves to also distribute the points randomly in space. In our implementation, the data are normalized so that $\sigma = 1$. For each test point, initially $\epsilon = \delta = 3\sigma$. The number of points in the δ-ball around the representative point $x(t_i)$ is n. Image points in the ball centered around the point $y(t_i)$ are counted; this number is m. Then the binomial distribution with parameters $(n, .5)$ is computed to find the cumulative probability of finding m or more image points in the ϵ-ball. If this probability is $< .05$, the null hypothesis is rejected for this point and ϵ is recorded as ϵ^*. Then ϵ is reduced with the same δ. If the null hypothesis is not rejected, δ is reduced. To maintain the 95% confidence interval, there must be at least 5 temporally non-correlated points in the δ-ball. If no ϵ can be found with *any* acceptable δ, we increase the initially allowed ϵ until ϵ^* can be found for all points. Note that ϵ^* for each point represents the *smallest* ϵ for which the null hypothesis is rejected. The average and distribution of ϵ^* is recorded, along with the maximum δ for each ϵ^*.

To detect differences in geometric structures using the continuity test, we compare both the average ϵ^* and the distribution of ϵ^* for the set of representative points. For comparison, we compute the continuity statistics for a known functional relationship in order to see the smallest possible ϵ ; call this value ϵ_0. If $\epsilon* \gg \epsilon_0$ for a particular test, it is clear that any functional relationship between the source and target attractors has degraded. If ϵ^* is close to ϵ_0, we examine the distribution for the tests in question and for the known relationship to detect either degradation of a functional relationship or evidence that a continuous functional relationship persists.

For example, if we are testing for a continuous function from the attractor reconstructed from one filtered signal to the attractor reconstructed from an identical signal with a different filter, we first look for ϵ^* values for a function between each attractor and itself. We call these ϵ_0. Then since the same input signal was used, we are able to test for a continuous function between attractors. Note that the same signal is necessary to use the continuity test with a time series embedding. Since points in a time delay embedding are assigned a time signature, a mapping exists between source and target points with the same time signature. We test to see if there is evidence that this map is continuous.

We emphasize that the continuity statistic is a one-sided statistic. Thus, evidence of a continuous functional relationship $f : X \to Y$ does not imply existence of a continuous function $g : Y \to X$. Those relationships must be tested separately. In practice, we compute the continuity statistic using source X and target Y and then compute the statistics using source Y and target X. These statistics are considered separately, but we note that in our tests, the continuity tests for both functional directions gave similar statistics.

0.4 Experiments

The experiments were performed by exciting a scaled three-story frame structure with a chaotic Lorenz oscillator. The test structure is constructed of aluminum Unistrut columns and aluminum floor plates. It is shown in figure 5. The floors were 1.3-cm thick aluminum plates with two bolt connections to brackets on the Unistrut columns. The base was as 3.8 cm thick aluminum plate. Support brackets for the columns were bolted to the floor plate. All bolted connections were tightened to a torque of 12.4 Nm in the undamaged state. Four Firestone airmount isolators allowed the structure to move freely in horizontal directions; these were bolted to the bottom of the base plate. The isolators were mounted on aluminum blocks and plywood so the base of the structure was level with the shaker. The isolators were inflated to 140 kPa. The shaker was connected to the structure by a 7.9 cm long, 9.5mm diameter stinger. The stinger was screwed into a tapped hole in the middle (both horizontally and vertically) of the 61 cm side of the structure's base plate to impart translational motion. On floor 1, 6 piezoelectric accelerometers were installed. These accelerometers were mounted on blocks glued to three of the Unistrut columns (Joints A, B and D) at the floor level in both in-plane directions. Sensor locations are shown in figure 6.The normal sensitivity of each accelerometer was 1 V/g. Additionally, a force transducer was mounted between the stinger and the base plate. This force transducer was used to measure the input to the base of the structure. A commercial data acquisition system controlled from a laptop PC was used to digitize the accelerometer's and force transducer's analog signals. The sensor and cabling were verified by using a handheld shaker to send a sine wave to each accelerometer separately in order to visually inspect the outputs for each channel. Tests to determine noise floor and sampling rate were done before any other tests were performed.

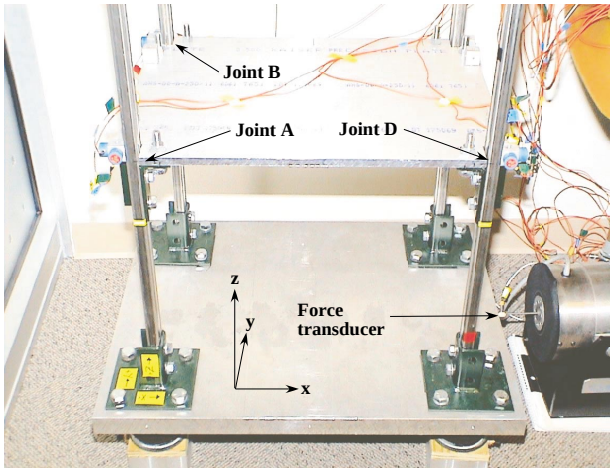

Figure 5: Experimental Apparatus

The input signal was a Lorenz oscillator. The generic system can be represented by the following:

$$\eta \dot{x}_1 = 16(x_2 - x_1) \tag{6}$$

$$\eta \dot{x}_2 = 40x_1 - x_2 + x_1 x_3 \tag{7}$$

$$\eta \dot{x}_3 = -4x_3 + x_1 x_2 \tag{8}$$

In this system of equations, the parameter η either speeds up or slows down the oscillation. Note that this controls the expansion

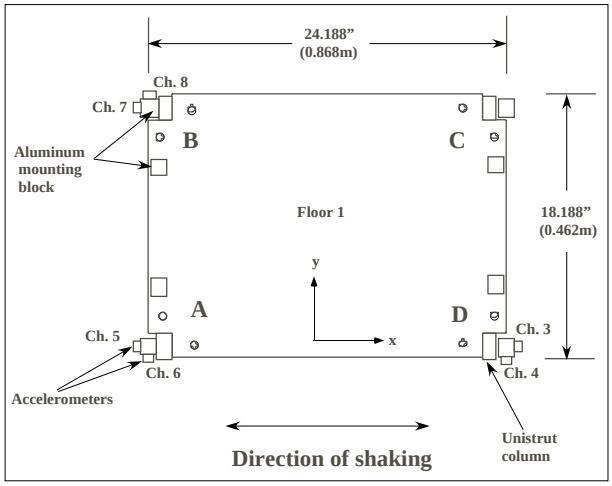

Figure 6: Sensor Locations

rates and ultimately the stability of the response. In this experiment, specifically we used the x_1 solution of the Lorenz to excite the structure.

The output signals consisted of an x-(parallel to the direction of shaking) and a y-(orthogonal to the direction of shaking) direction signal at each joint. We also measured the signal at the transducer.

The Lyapunov exponents of the drive signal are calculated as an expansion rate, that is, in units of sec^{-1}.If the playback rate of the signal is increased (the data rate increased) we note that the expansion rate also increases. Thus, the expansion rates of the entire system depend on the data rate of the drive (input) signal as well as on the characteristic exponents of the linear filter.

One measure of the fractal dimension of the underlying attractor is directly related to the Lyapunov exponents via the Kaplan-Yorke conjecture [9]. This, in turn, affects the geometry of the attractor. If the Lyapunov exponents of the drive signal are changed by the data rate, the dimensionality of the entire attractor is affected. In these experiments, we used two data rates and measured geometric differences in the underlying attractors for both data rates.

0.5 Application of the Continuity Test

A false nearest-neighbor analysis of the output data from the structure experiments showed that the output signals at each of the joint sensors did not require addition of data from other joints' sensors in order to adequately embed the time series. Thus, it was conjectured that there might be continuous functions between the phase-spaces constructed by embedding the time series from the joints alone. After a false nearest neighbor analysis of each of the joints' x-component time series, we determined that those phase spaces could be adequately reconstructed in dimension 3. To obtain time-delay for each of the x-component time series, we examined the autocorrelation functions for those time series. The time delay for data rate 2 was 75 and the time delay for data rate 3 was 650.

We performed the continuity test on each pair of time-series reconstructions in the undamaged scenario (scenario 0) and found evidence of continuous functions between all 3 joints' phase-space reconstructions. This ev-

idence is presented in figures 10- 39. In the undamaged scenario, the average ϵ^* was close to .3 in both data rate 2 and data rate 3 tests. The distribution of ϵ^* for a representative scenario 0 test is show in figure 13.

We then performed the continuity test between pairs of joints' phase-space reconstructions in the other 5 scenarios. We stress that on the other 5 scenarios, these were *blind tests* in that we did not know either the location or severity of damage, if any, at the time of the tests. In all continuity tests, we utilized a Theiler Window of 100 time steps in order to limit false spatial correlations between points that are temporally correlated. For an explanation of the Theiler Window, see e.g. [21]. We tested continuity for all pairs in both directions. The results are displayed in figures 10-39. The degree to which continuity was lost was dependent both on scenario and on data rate. We note that continuity was tested for both directions (e.g. from joint A to joint B and from joint B to joint A) but the results were quite similar for both. For clarity, only one direction appears in the plots.

0.6 Results

Looking at figures 10-39, we consider the continuity statistic for damage scenarios 1-5. Information from scenario 0 (undamaged scenario) appears on the graphs for comparison. For simplicity, let ϵ_0 be the largest ϵ^* obtained in the undamaged scenarios, where comparison is only made for the continuity test between the same joints (e.g. we compare ϵ^* for scenario 1, continuity between joints A and D to ϵ_0 for scenario 0, continuity between joints A and D only).We refer to figures 8 and 9. These tables summarize the performance of the continuity test in damage prediction and localization for each scenario and the two tested data rates.

0.6.1 Scenario 1

First we focus on figures 10- 15. They show that average $\epsilon* \gg \epsilon_0$ for the maps between joints D and A and D and B. In these graphs, we also see no overlap at all in the 94% confidence interval for $\epsilon*$ versus the 94% confidence interval for ϵ_0. For the map between joints A and B, we see that average $\epsilon* > \epsilon_0$, but that the confidence intervals do overlap both for data rate 2 and data rate 3. One could conclude that it is clear that joint D is definitely damaged (from the loss of continuity of maps between joint D and joint A and joint D and joint B) and other joints may or may not be damaged, but there is not overwhelming evidence that either joint B or joint A is damaged. Thus, we conclude that joint D only is damaged in this scenario.

0.6.2 Scenario 2

Next we consider scenario 2. Those graphs appear in figure 16-21. In all three of the data rate 2 graphs, we see average $\epsilon* > \epsilon_0$ and a clear shift of the 94% confidence interval to larger $\epsilon*$. This leads us to conclude that damage has occurred, but there is no overwhelming evidence that indicates any one joint is damaged. However, we see in the graphs for data rate 3 (figures 19 and 21)

that $\epsilon* \gg \epsilon_0$ for continuity between joints D and A and between joints A and B, with 94% confidence intervals completely disjoint from those of scenario 0. This is sufficient evidence to conclude that joint A is damaged. However, ambiguous results for data rate 2 and some elevation of $\epsilon*$ over ϵ_0 for continuity between joint D and joint B in data rate 3 do not allow us to conclude that no other joint is damaged in this scenario.

0.6.3 Scenario 3

Scenario 3 shows some very clear evidence of damage only to Joint B. The graphs for this scenario are shown in figures 22-27. In figure 24 we see nearly identical confidence intervals for continuity between joints D and A; in this case we have average $\epsilon* \approx \epsilon_0$. However, the graphs for the maps between joints D and B and between joints A and B show no overlap at all of the 94% confidence intervals, and average $\epsilon* \gg \epsilon_0$. The same results appear for data rate 3, although we see some slight elevation of $\epsilon*$ over ϵ_0 for continuity between joints D and A. However, the change in the distribution is slight compared to the differences in confidence intervals for the other functional relationships. Thus we conclude that joint B only is damaged in this scenario.

0.6.4 Scenario 4

The graphs for scenario 4, shown in figures 28 -32 show clear evidence of damage. In all three graphs, we see average $\epsilon* \gg \epsilon_0$ and little or no overlap of the 94% confidence intervals for continuity of maps between all three joints. Thus, we conclude that damage has occurred, and it is likely that it has occurred in more than one joint. The data rate 3 results, seen in figures 29, 31 and 33 substantiate this claim; in all three functional relationships we see $\epsilon* \gg \epsilon_0$ and no overlap of the 94% confidence intervals.

0.6.5 Scenario 5

We next consider scenario 5. These graphs appear in figures 34-39. In all of these graphs, we see average $\epsilon* > \epsilon_0$, but no real separation of the 94% confidence intervals. In all of the graphs, we see a clear shift of the distribution to larger $\epsilon*$ for maps between joints in scenario 5; note that the lower end of the 94% confidence interval is clearly above average ϵ_0 for maps between joints D and A and between joints D and B. Thus, we can say conclusively that damage has occurred. However, there is no clear location of the damage. Considering data rate 3, in figures 35, 37 and 39, we have a bit of a contradiction. In all the other scenarios, differences between $\epsilon*$ and ϵ_0 were much larger for data rate 3 than they were for data rate 2. However, for this scenario, the difference between average $\epsilon*$ and ϵ_0 we saw for continuity between joints A and B in data rate 2 nearly disappeared in data rate 3. The data rate 2 results point to no clear location of damage, while the data rate 3 results point quite specifically to damage in joint D but no damage to either joint A or joint B.

Although the original continuity tests were blind tests, disclosure of the damage levels revealed that all 3 joints were unbolted in this scenario. It is possible that bouncing motion

was replaced by sliding motion because no bolts remained in the joints. Although the results clearly pointed to some sort of damage in this scenario, it is possible that the response of the structure to the applied vibration was quite different in this scenario than in the others. Certainly, further investigation of this sort of damage is indicated from the results of this experiment.

0.7 Conclusion

The continuity test clearly was able to detect damage in all 5 damage scenarios. In the scenarios that involved damage to joint D only or joint B only, the test was able to localize the damage for both data rates. Scenario 2 clearly showed evidence of damage, but localization was only marginally predictable and relied on only results from data rate 3. The other one-joint damage scenarios showed evidence of localization for both data rates. Scenario 4 also showed clear evidence of damage, but this test was not able to localize the damage. Scenario 5 posed something of a problem. All tests indicated that damage to joint D occurred. However, results were contradictory concerning damage to the other joints. For data rate 3, there was clear evidence that joints A and B were not damaged, while in data rate 2 there was some evidence of damage to joints A and B.

One of the drawbacks to this particular test was that we could not directly compare the attractors reconstructed from undamaged structures to those reconstructed from damaged structures. If the prerecorded signals were synchronized for each damage scenario in the frame structure tests it would be possible to match filtered signals to each other via the input signal. In this case, it would be possible to test for a continuous map between known undamaged responses and the responses for different damage scenarios (i.e. mapping undamaged reconstructions to damaged reconstructions). By comparing ϵ^* for maps between undamaged joints in different trials to ϵ^* for maps between an undamaged and a damaged joint it might be possible to localize damage for the scenarios that exhibited damage to more than one joint. In [11] this method, using identical prerecorded signals on both damaged and undamaged structures, identification of very low levels of damage was possible using the continuity test. However, damage in those experiments was confined to one location in the structure; localization was not discussed.

The continuity test warrants further investigation as a tool both to detect and to localize damage. One advantage to the continuity test is that the output does not require additional statistical analysis other than scrutiny of the distribution of the $\epsilon*$. Thus it is possible to set a threshold above which elevated average $\epsilon*$ could signal damage; this would allow a certain degree of automation in the damage detection process. It is especially encouraging that conclusive results were obtained for 4 out of 5 scenarios even in a blind-test environment.

Scenario	Joint A	Joint B	Joint D
0	none	none	none
1	none	none	bolts removed
2	bolts removed	none	none
3	none	bolts removed	none
4	bolts removed	none	bolts removed
5	bolts removed	bolts removed	bolts removed

Figure 7: Damage Scenarios

Scenario	Actual Damage			Detected Damage		
	A	B	D	A	B	D
1	N	N	Y	N	N	Y
2	Y	N	N	Y	Y	Y
3	N	Y	N	N	Y	N
4	Y	N	Y	Y	Y	Y
5	Y	Y	Y	Y	Y	Y

Figure 8: Damage Classification Results, Data Rate 2. Actual Damage follows figure 7

Scenario	Actual Damage			Detected Damage		
	A	B	D	A	B	D
1	N	N	Y	N	N	Y
2	Y	N	N	Y	Y	Y
3	N	Y	N	N	Y	N
4	Y	Y	N	Y	Y	Y
5	Y	Y	Y	N	N	Y

Figure 9: Damage Classification Results, Data Rate 3. Actual Damage follows figure 7

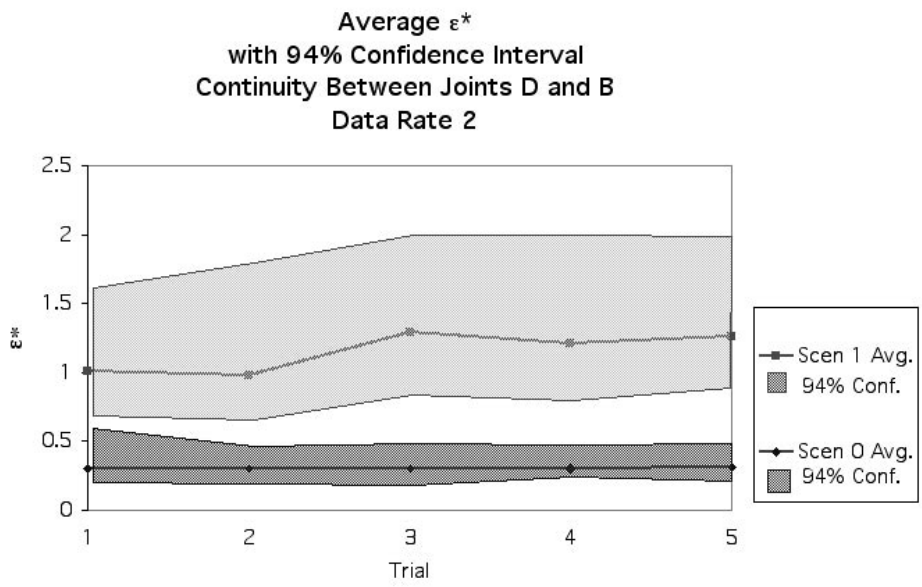

Figure 10: Scenario 1, Data Rate 2.

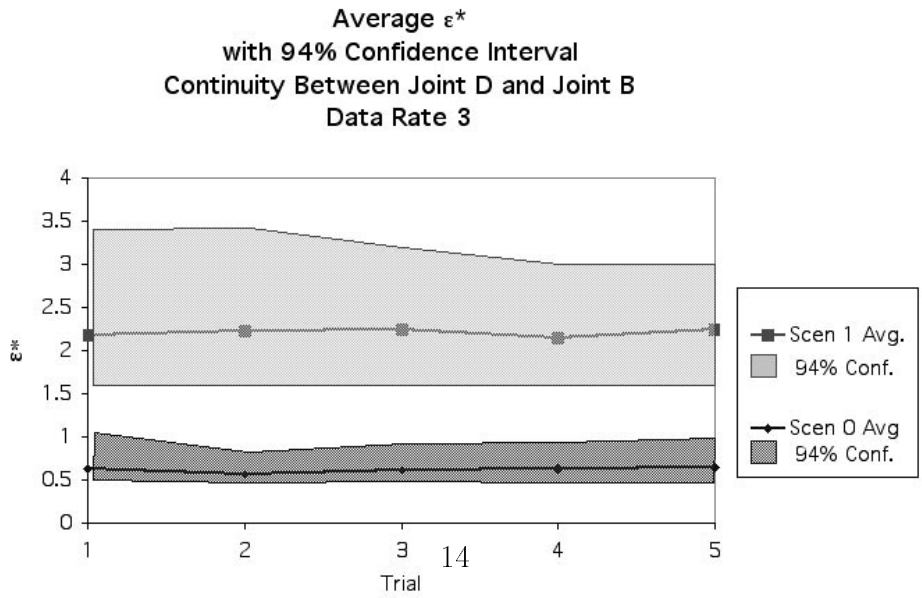

Figure 11: Scenario 1, Data Rate 3.

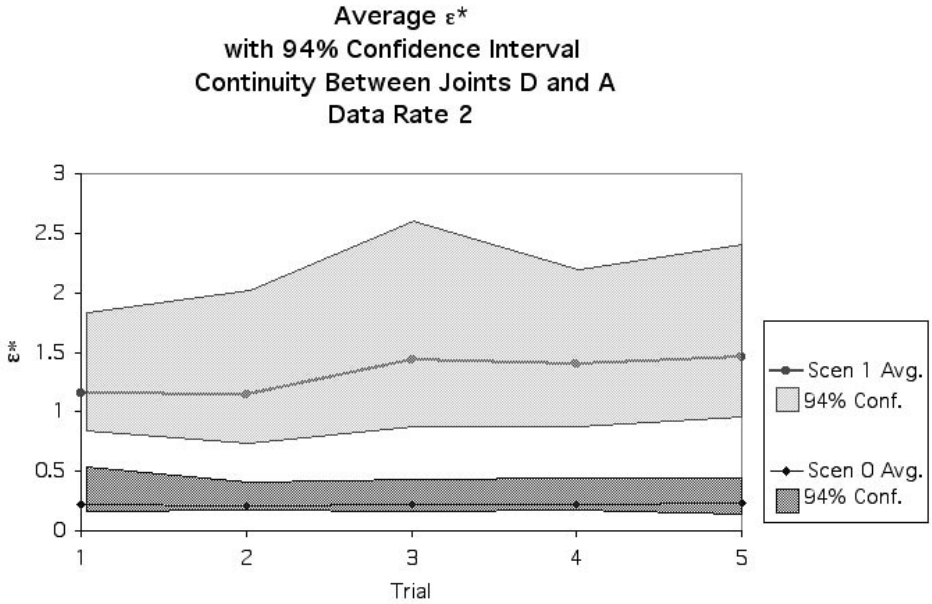

Figure 12: Scenario 1, Data Rate 2.

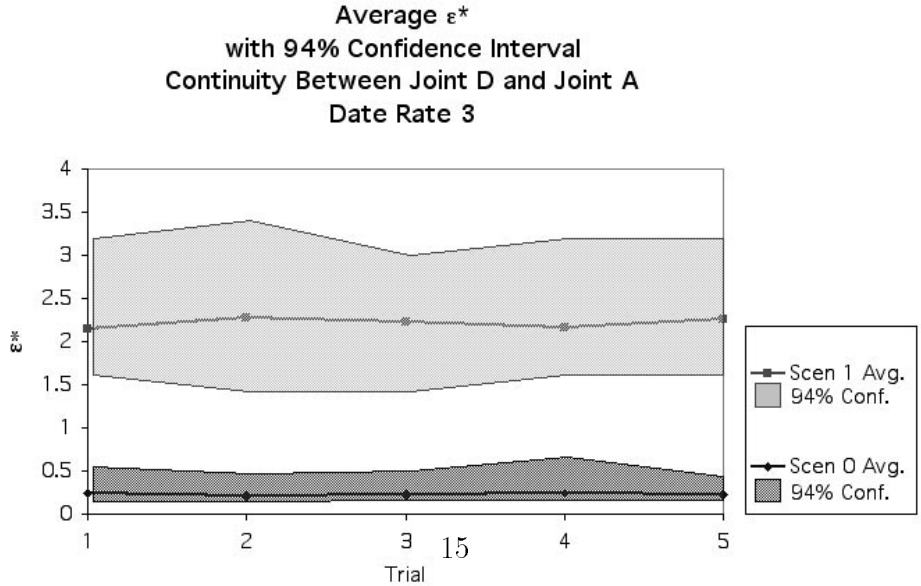

Figure 13: Scenario 1, Data Rate 3.

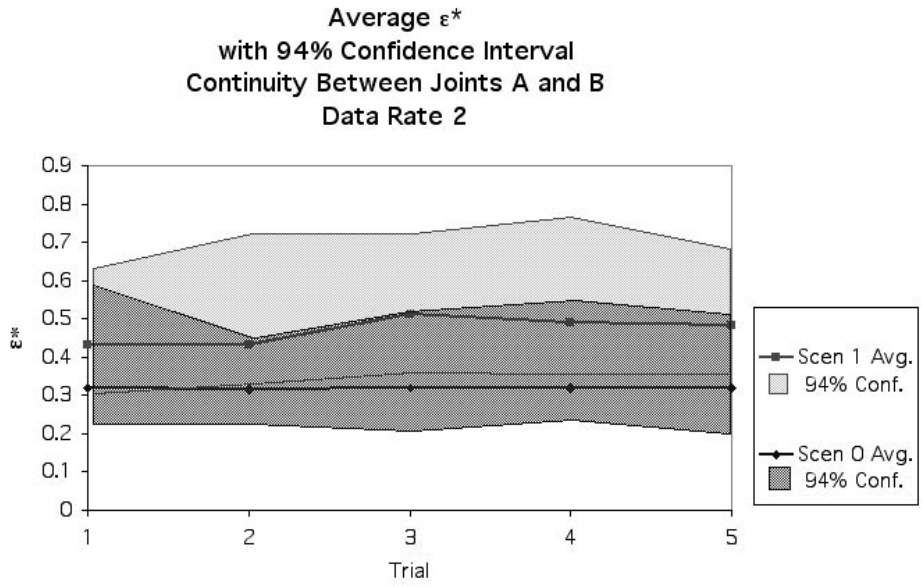

Figure 14: Scenario 1, Data Rate 2.

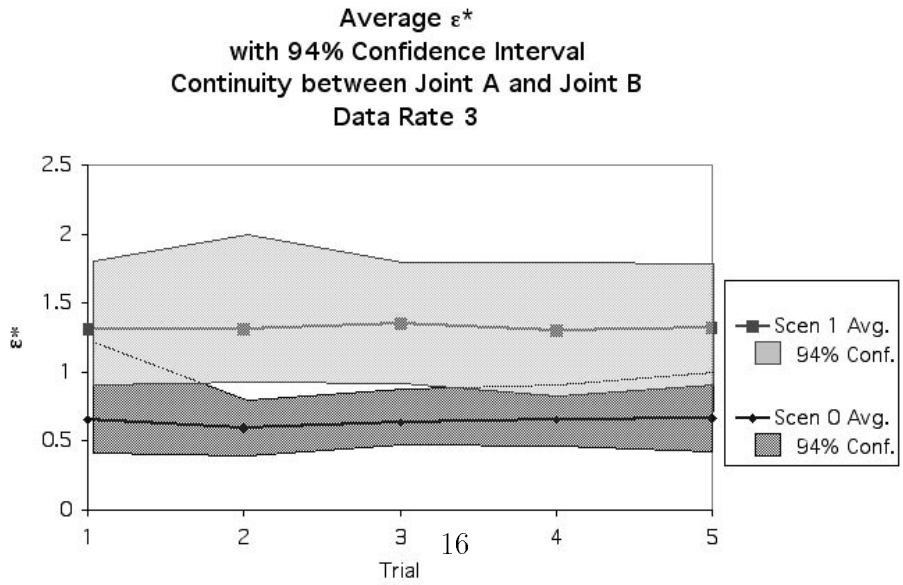

Figure 15: Scenario 1, Data Rate 3.

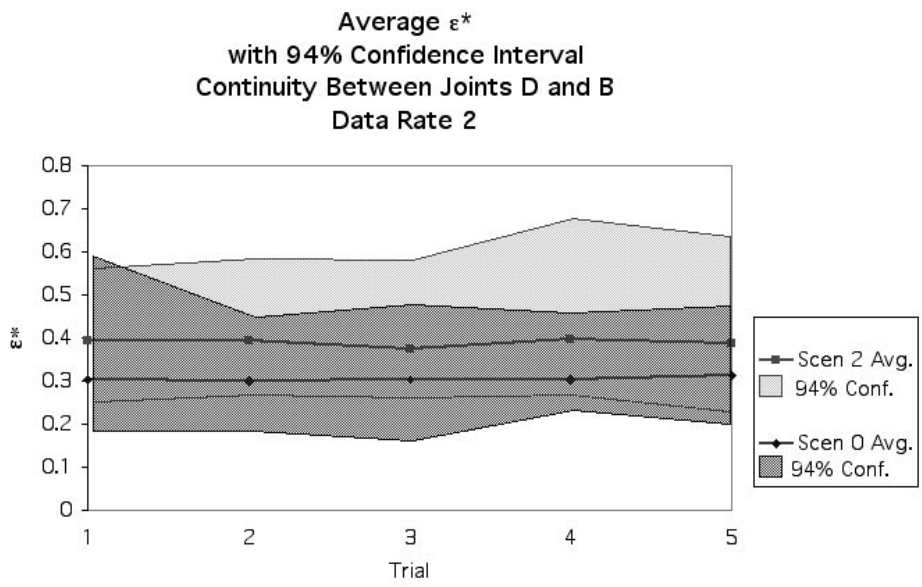

Figure 16: Scenario 2, Data Rate 2.

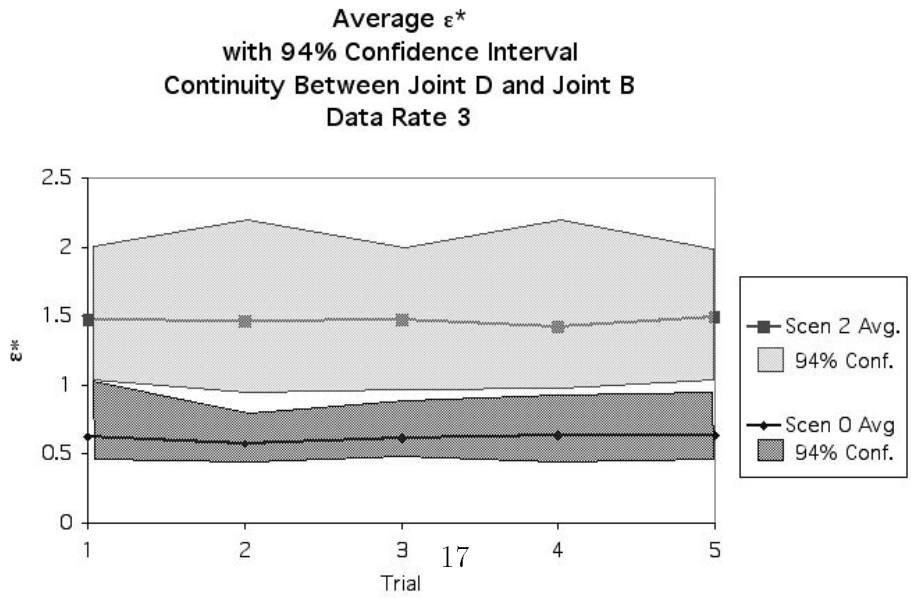

Figure 17: Scenario 2, Data Rate 3.

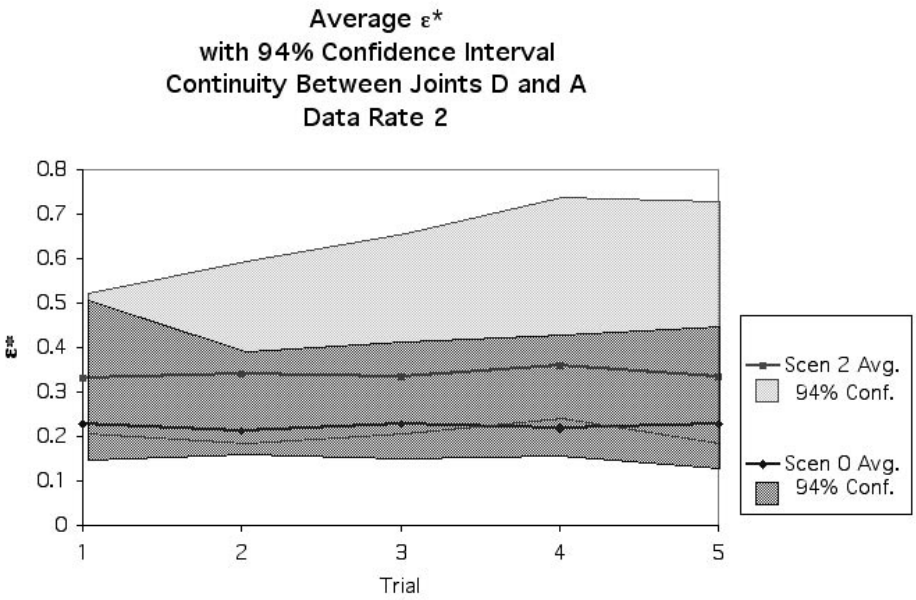

Figure 18: Scenario 2, Data Rate 2.

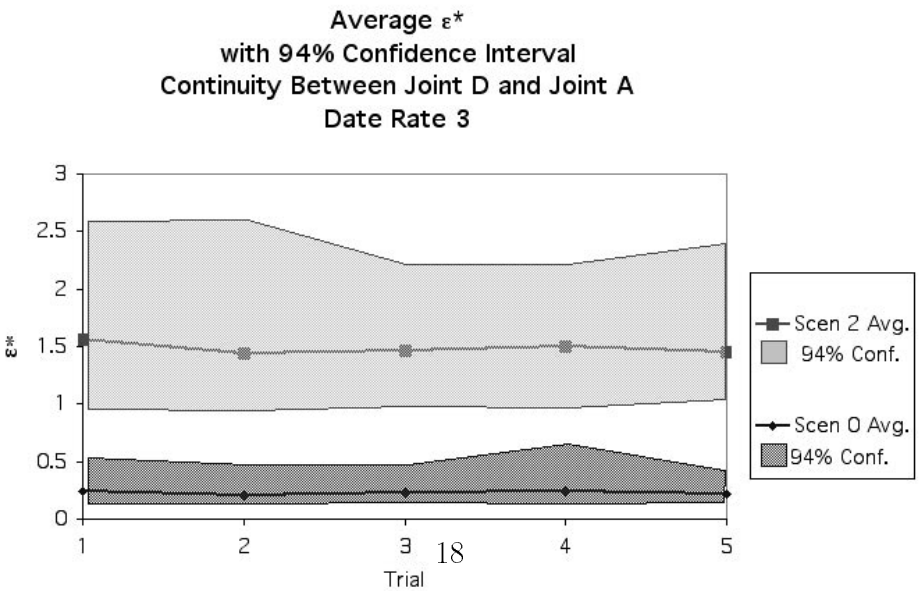

Figure 19: Scenario 2, Data Rate 3.

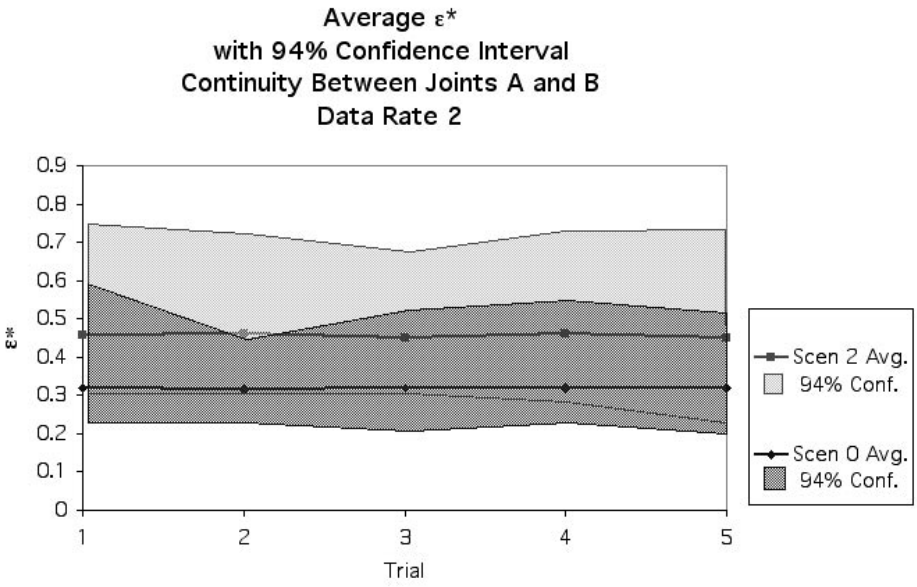

Figure 20: Scenario 2, Data Rate 2.

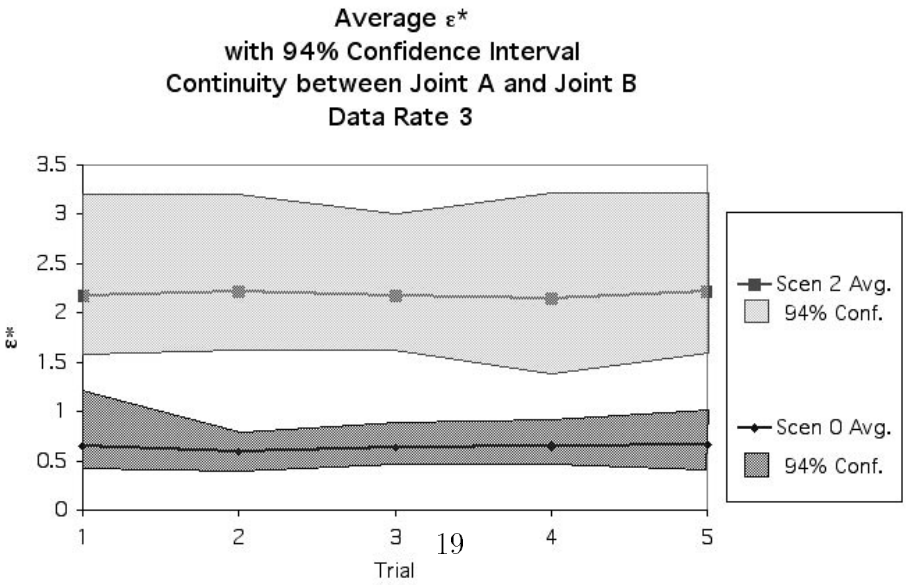

Figure 21: Scenario 2, Data Rate 3.

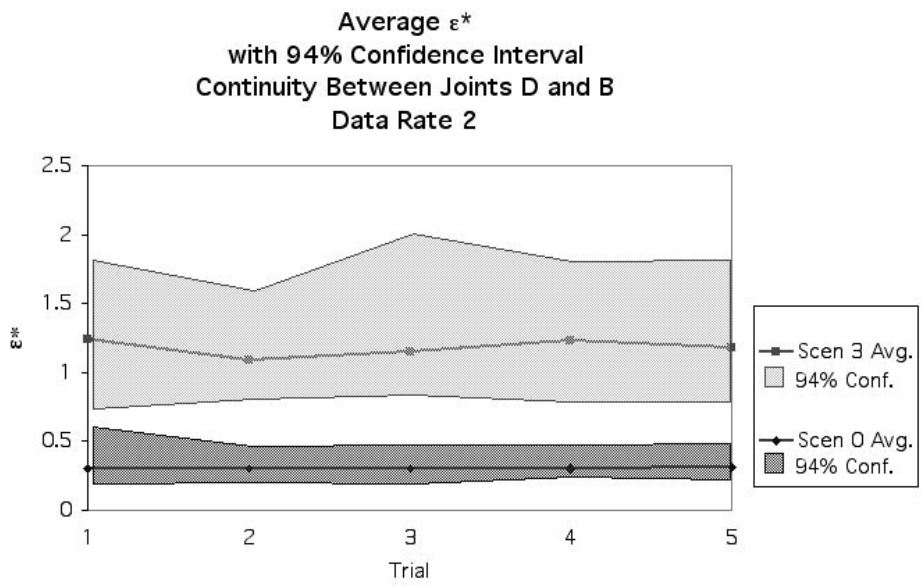

Figure 22: Scenario 3, Data Rate 2.

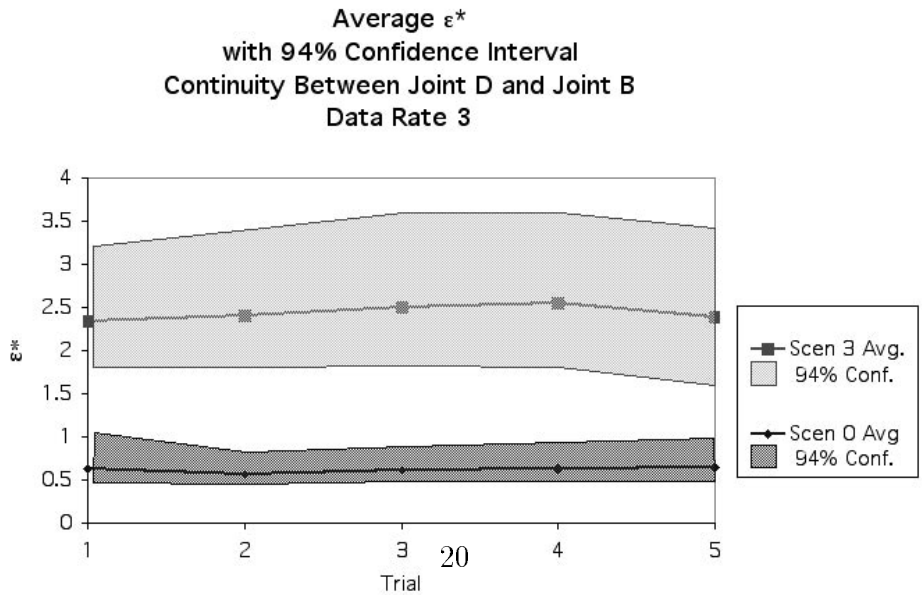

Figure 23: Scenario 3, Data Rate 3.

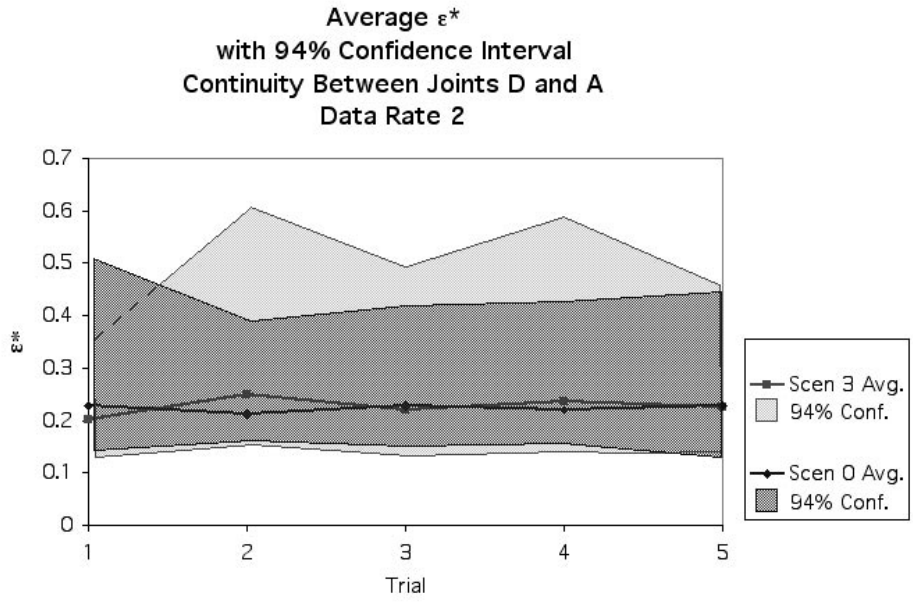

Figure 24: Scenario 3, Data Rate 2.

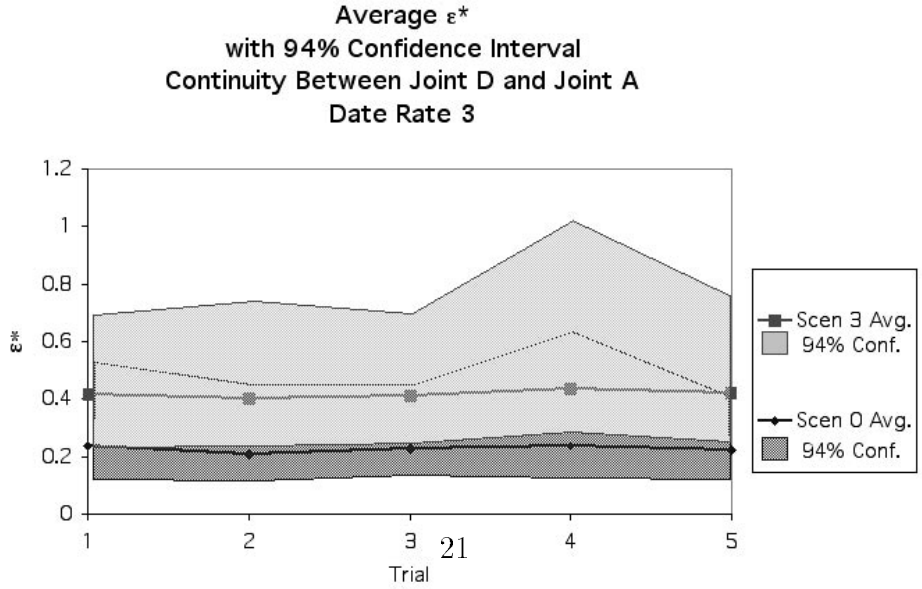

Figure 25: Scenario 3, Data Rate 3.

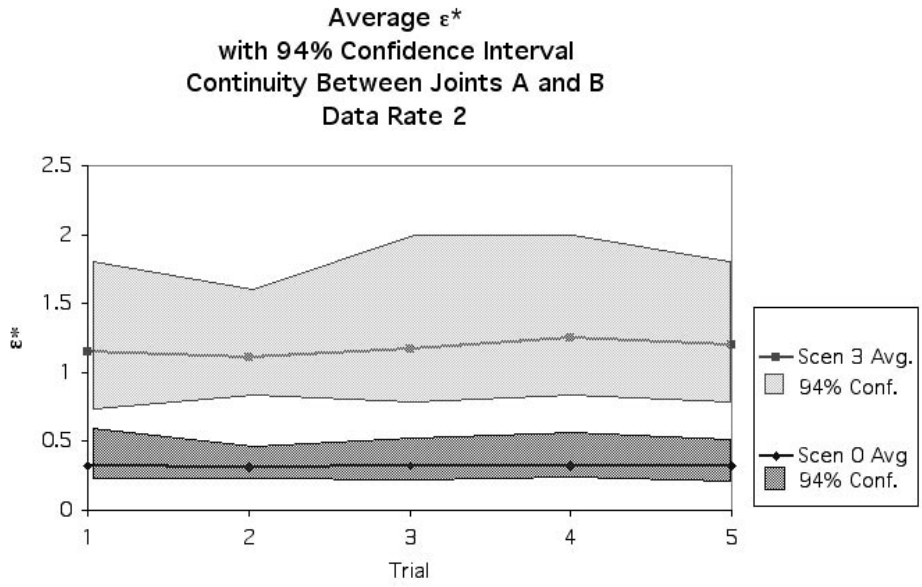

Figure 26: Scenario 3, Data Rate 2.

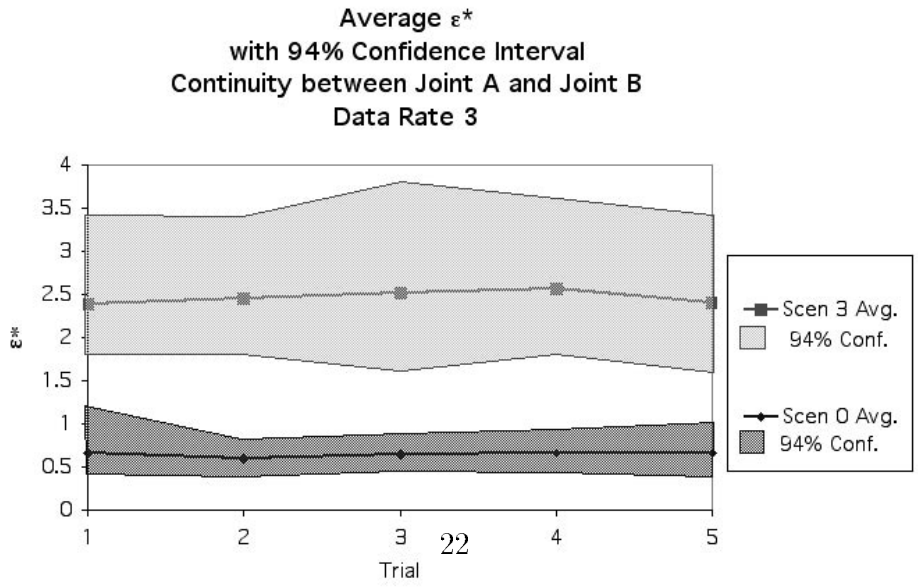

Figure 27: Scenario 3, Data Rate 3.

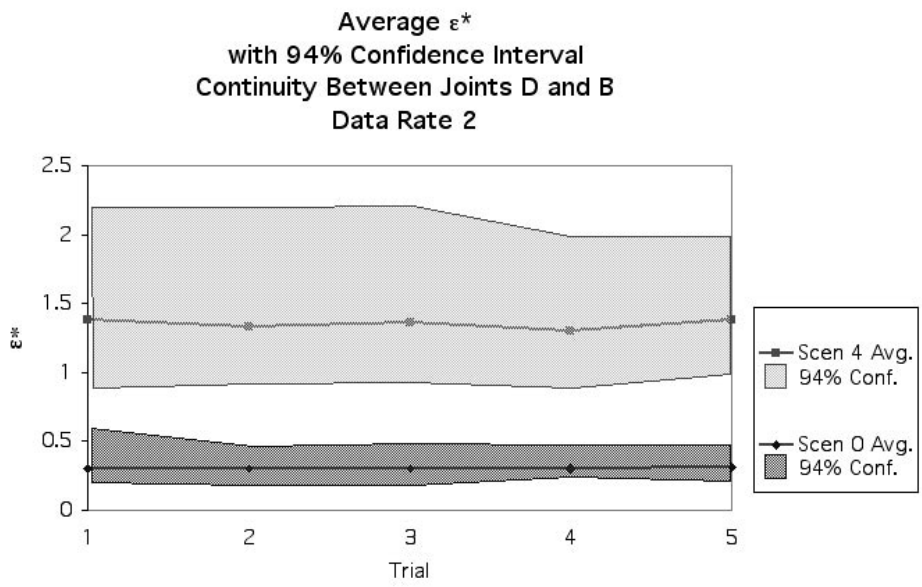

Figure 28: Scenario 4, Data Rate 2.

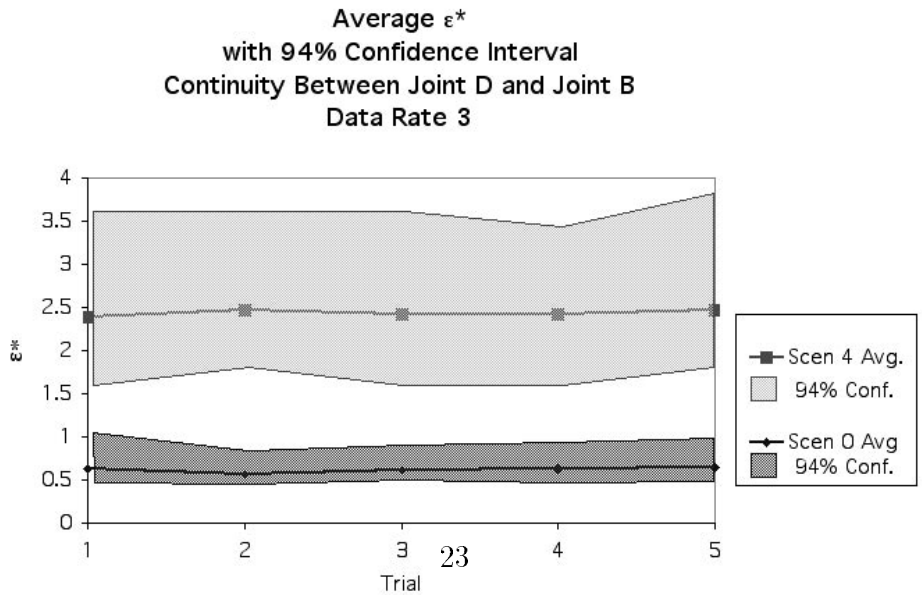

Figure 29: Scenario 4, Data Rate 3.

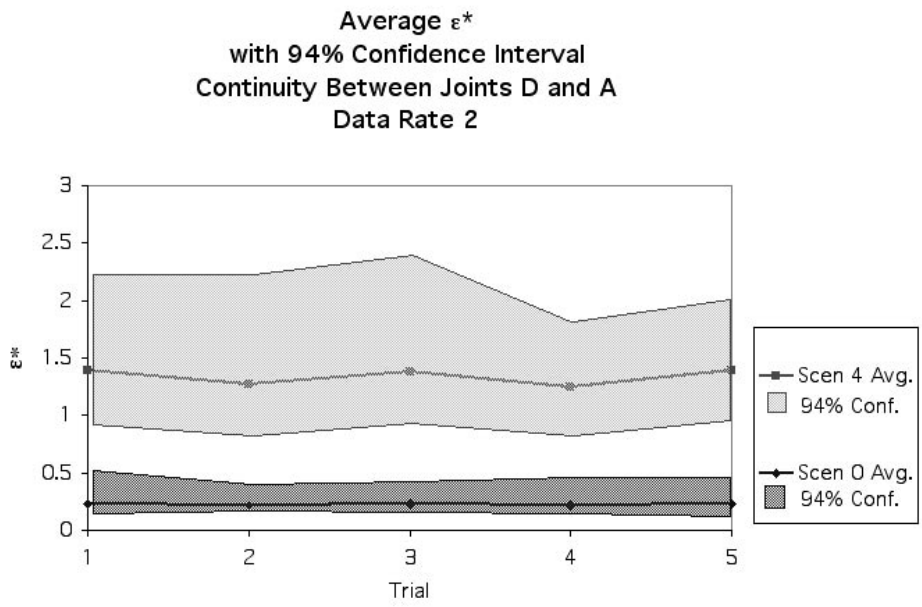

Figure 30: Scenario 4, Data Rate 2.

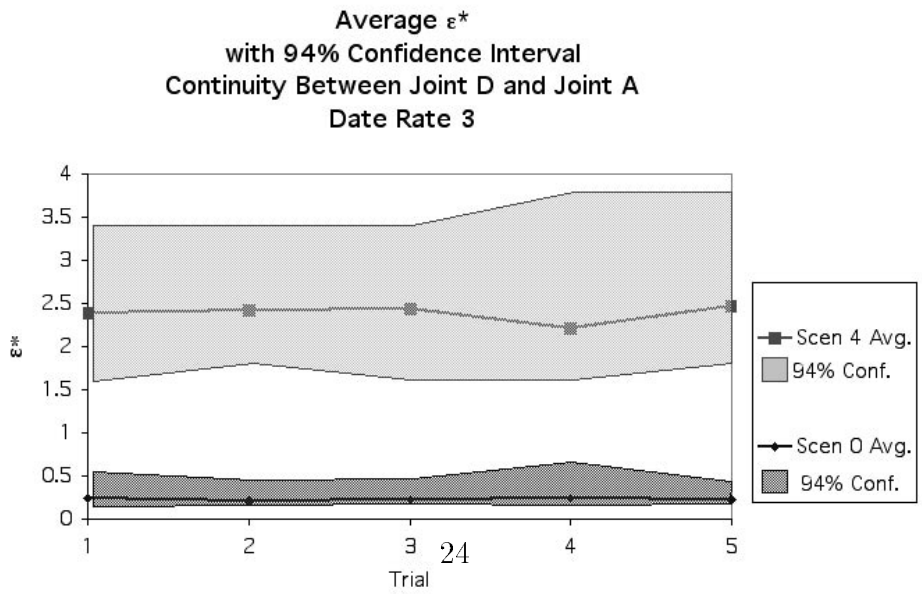

Figure 31: Scenario 4, Data Rate 3.

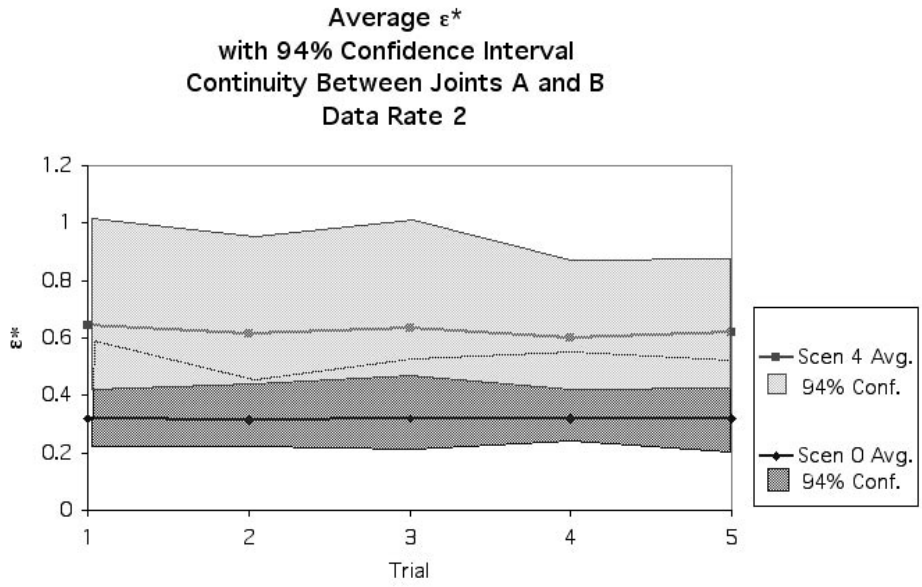

Figure 32: Scenario 4, Data Rate 2.

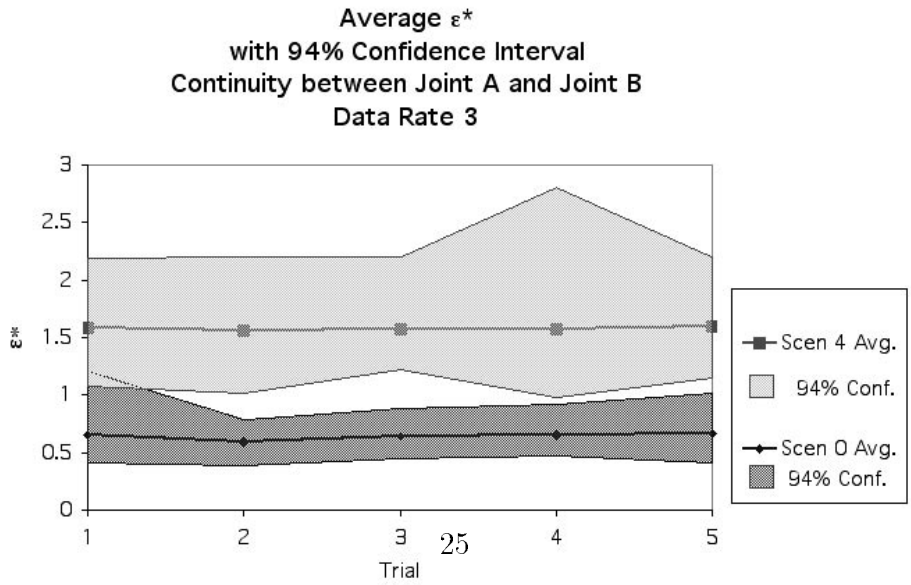

Figure 33: Scenario 4, Data Rate 3.

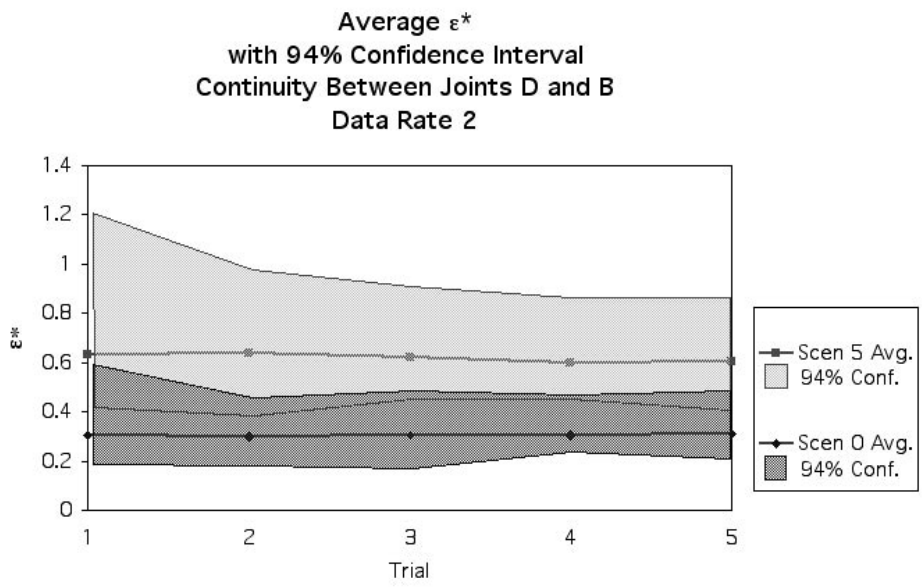

Figure 34: Scenario 5, Data Rate 2.

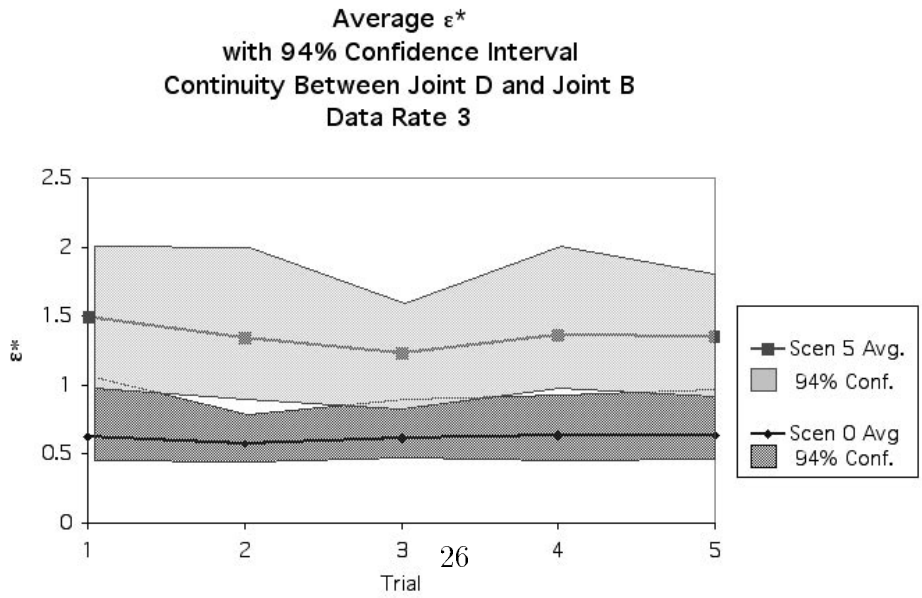

Figure 35: Scenario 5, Data Rate 3.

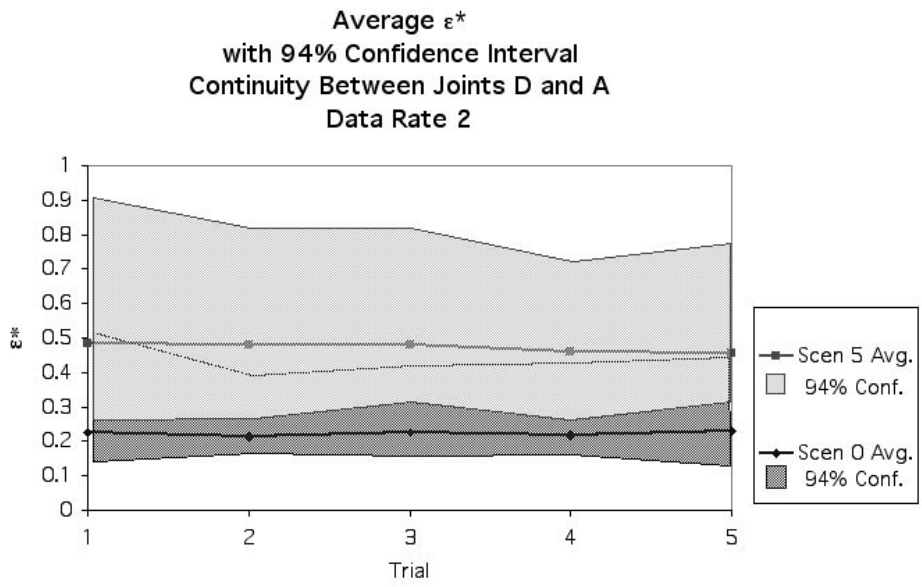

Figure 36: Scenario 5, Data Rate 2.

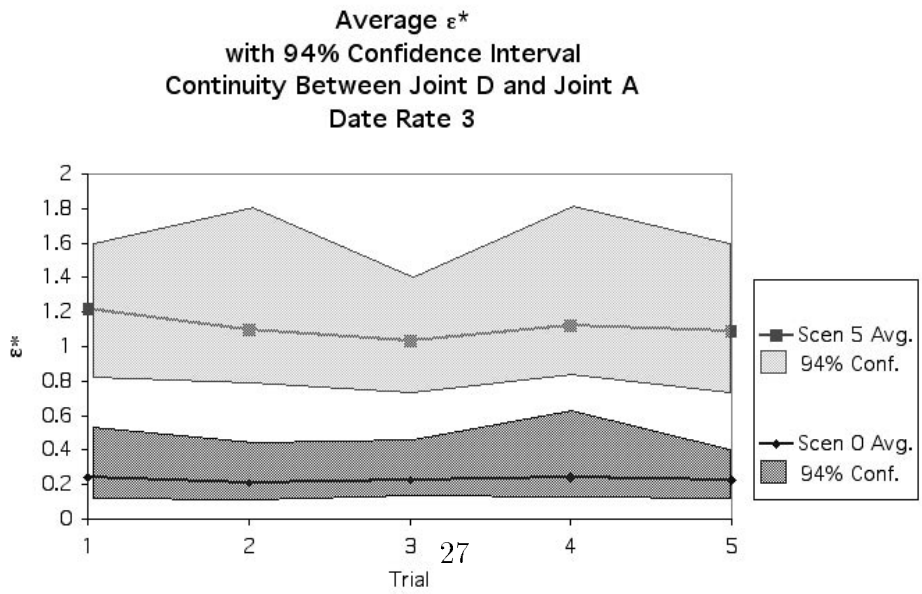

Figure 37: Scenario 5, Data Rate 3.

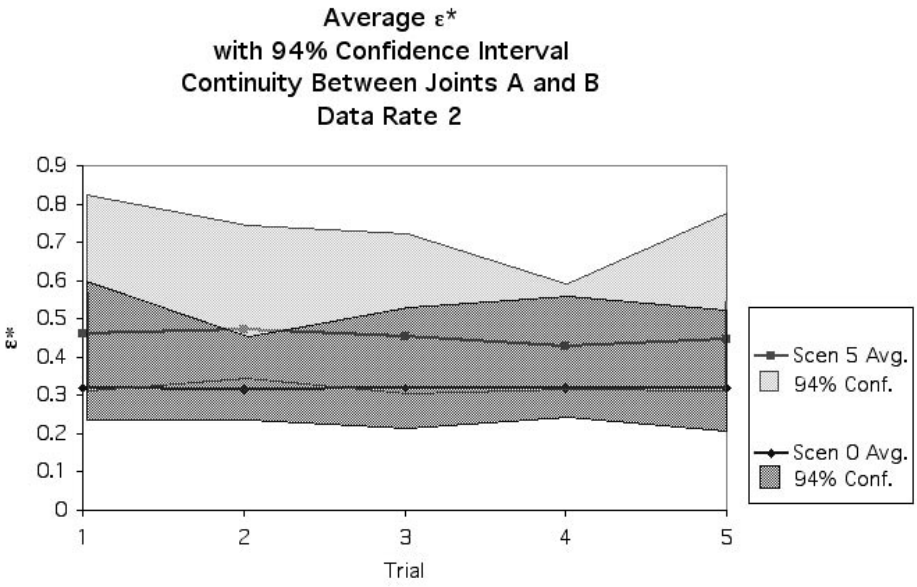

Figure 38: Scenario 5, Data Rate 2.

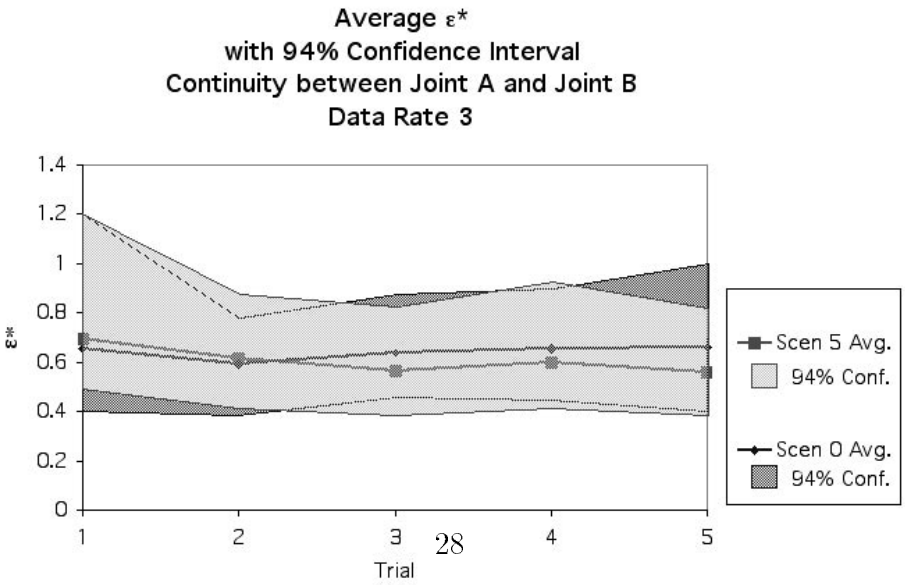

Figure 39: Scenario 5, Data Rate 3.

Bibliography

[1] H T Banks, M L Joyner, B Wincheski, and W P Winfree. Real time computational algorithms for eddy-current based damage detection. *Inverse Problems*, 18:795–823, 2002.

[2] S. Boccaletti, D.L. Valladares, L.M. Pecora, H. P. Geffert, and T. L. Carroll. Reconstructing embedding spaces of coupled dynamical systems from multivariate data. *Physical Review E*, 65, 2002.

[3] K.M. Campbell and M.E. Davies. The existence of inertial functions in skew product systems. *Nonlinearity*, 9:801–817, 1996.

[4] M.E. Davies and K.M. Campbell. Linear recursive filters and nonlinear dynamics. *Nonlinearity*, 9:487–499, 1996.

[5] J.E. Doherty. Nondestructive evaluation. In A.S. Kobayashi, editor, *Handbook on Experimental Mechanics*, chapter 12. Society for Experimental Mechanics, Englewood Cliffs, New Jersey, 1987.

[6] C R Farrar, T A Duffey, S W Doebling, and D A Nix. A statistical pattern recognition paradigm for vibration-based structural health monitoring. *Structural Health Monitoring 2000*, 1999.

[7] A. Fraser and H. Swinney. Independent coordinates for strange attractors from mutual information. *Physical Review A*, 33(2):1134–1140, 1986.

[8] J.M.Nichols, M.D.Todd, M.Seaver, and L.N.Virgin. Use of chaotic excitation and attractor property analysis in structural health monitoring. *Phys Rev E*, 67(016209), 2003.

[9] J. Kaplan and James A. Yorke. *Lecture Notes in Math*, volume 730, chapter Chaotic behavior of multidimensional difference equations, pages 228–237. Springer:Berlin, 1979.

[10] M. Kennel, R. Brown, and H. Abarbanel. Determining embedding dimension for phase-space reconstruction using a geometrical construction. In Ott, Sauer, and Yorke, editors, *Coping with Chaos*. Wiley, 1994.

[11] L.J. Moniz, L.M. Pecora, T.L. Carroll, M.D. Todd, S. Trickey, and J. Nichols. Vibration-based damage assessment using novel function statistics with multiple time series. In S. Boccaletti, T. Carroll, B. Gluckman, L. Kocarev, V. In, and J. Kurths, editors, *Proceedings of the 7th Experimental Chaos Conference*. American Institute of Physics, 2002.

[12] A K Pandey and M Biswas. Damage detection in structures using changes in flexibility. *Journal of Sound and Vibration*, 169:3–17, 1994.

[13] L.M. Pecora. Using multiple time series correctly. In S. Boccaletti, T. Carroll, B. Gluckman, V. In, L. Kocarev, and J. Kurths, editors, *Proceedings of the 7th Experimental Chaos Conference*. American Institute of Physics, 2002.

[14] L.M. Pecora, T.L. Carroll, and J.F. Heagy. Statistics for continuity and differentiability: An application to attractor reconstruction from time series. *Fields Institute Communications*, 11, 1997.

[15] R P Sampaio, N M N Maia, and J M M Silva. Damage detection using the frequency-response-function curvature method. *Journal of Sound and Vibration*, 226:0129–1042, 1999.

[16] Tim Sauer, James A. Yorke, and Martin Casdagli. Embedology. *Journal of Statistical Physics*, 65(3/4):579–616, 1991.

[17] J K C Shih, R Delpak, C W Hu, P Plassman, A Wawrzynek, and M Kogut. Thermographic nondestructive testing damage detection for metals and cementitious materials. *Imaging Science Journal*, 48:33–43, 2000.

[18] H Sohn, C R Farrar, N F Hunter, and K Worden. Structural health monitoring using statistical pattern recognition techniques. *Journal of Dynamic Systems, Measurement and Control*, 123:706–711, 2001.

[19] M J Sundaresan, A Ghoshal, and M J Schulz. A continuous sensor for damage detection in bars. *Smart Materials and Structures*, 11:475–488, 2002.

[20] N Takeda. Characterizaiton of microscopic damage in composite laminates and real-time monitoring by embedded optical fiber sensors. *International Journal of Fatigue*, 24:281–289, 2002.

[21] J. Theiler. Spurious dimension from correlation algorithms applied to limited time-series data. *Physical Review A*, 34(12):2427–2431, 1986.

[22] M.D. Todd, J.M. Nichols, L.M. Pecora, and L.N. Virgin. Vibration-based damage assessment utilizing state-space geometry changes: Local attractor variance ratio. *Smart Materials and Structures*, 10:1000–1008, 2001.

[23] D Tuzzeo and di Scalea FL. Non-contact air-coupled ultrasonic guided waves for detection of hidden corrosion in aluminum plates. *Journal of Research in Nondestructive Evaluation*, 13:61–78, 2002.

[24] P Verboven, E Parloo, P Guillaume, and M V Overmeire. Autonomous structural health monitoring = part i; modal parameter estimation and tracking. *Mechanical Systems and Signal Processing*, 16:637–657, 2002.

[25] J.A. Yorke and H. Nusse. Dynamics 2. Springer-Verlag, 1998. Computer Program.